

Wetting on smooth micropatterned defects

Damien Debuissou, Renaud Dufour, Vincent Senez and Steve Arscott*

*Institut d'Electronique, de Microélectronique et de Nanotechnologie (IEMN),
University of Lille, CNRS UMR-8520, Cite Scientifique, Villeneuve d'Ascq, France.*

We develop a model which predicts the contact angle hysteresis introduced by smooth micropatterned defects. The defects are modeled by a smooth function and the contact angle hysteresis is explained using a tangent line solution. When the liquid micro-meniscus touches both sides of the defect simultaneously, depinning of the contact line occurs. The defects are fabricated using a photoresist and experimental results confirm the model. An important point is that the model is *scale-independent*, i.e. the contact angle hysteresis is dependent on the aspect ratio of the function, not on its absolute size; this could have implications for natural surface defects.

PACS numbers: 68.08.Bc, 47.55.D-, 85.40.Hp

Complex wetting [1-5] is observed on both natural [6-8] and artificial [2,5,9] surfaces. When a sessile droplet contracts (e.g. via evaporation) or swells (e.g. via condensation) the contact line (i.e. the liquid-vapor-solid interface) can move. The contact angle hysteresis [3,10-13] is defined as the difference between the advancing contact angle (i.e. the contact line moving forwards) and the receding contact angle (i.e. the contact line moving backwards) and remains a poorly understood phenomenon. Here we show that the contact angle hysteresis introduced by a “smooth, regular” [4,12] defect can be successfully predicted using a simple *scale-independent* geometrical model. Contact angle hysteresis tuning could be fundamental for modern applications such as *inter alia* self-cleaning surfaces [14], miniaturized chemistry [15], self-assembly [16] and nanotechnology [17].

We consider here the contact angle hysteresis introduced by a smooth defect [4,12]. We assume that the defect can be modeled by a function $h(x)$ which is smooth in the mathematical sense i.e. it is differentiable. Fig. 1 illustrates the four possible cases considered here.

Figure 1(a) is an *advancing* contact line moving from left to right which encounters a smooth defect where the micro-meniscus *does not touch* the right hand side (r.h.s.) of the defect as the contact line moves over the defect. Fig. 1(b) is an *advancing* contact line, again moving from left to right, which encounters a smooth defect where the micro-meniscus *does touch* the r.h.s. of the defect. Fig. 1(c) is a *receding* contact line moving from right to left which encounters a smooth defect where the micro-meniscus *does not touch* the left hand side (l.h.s.) of the defect. Fig. 1(d) is a *receding* contact line moving from right to left which encounters a smooth defect where the micro-meniscus *does touch* the l.h.s. of the defect. In all cases the centre of the droplet is considered to be to the left of the defect. We consider that far from the defect the moving contact line has a receding or an advancing contact angle [4,12] given by $\theta_{r,a}$ and we define the *effective* receding and advancing contact angles $\theta_{r,a}^*$ as the contact angle when the contact line depins from the defect. Let us now consider the case of the receding contact angle in more detail, although it will be seen that the arguments apply equally to the

advancing contact angle via the symmetry of the defect considered here. As the contact line moves from right to left far from the defect, it does so with a contact angle equal to the receding contact angle θ_r . As the contact line moves down the r.h.s. ($x > 0$) of the defect, θ_r is maintained locally (in keeping with Young-Dupré equation [18,19]) but as we have seen the macroscopic contact angle reduces. It is important now to make a physical distinction between the liquid micro-meniscus touching the l.h.s. ($x < 0$) of the defect or not.

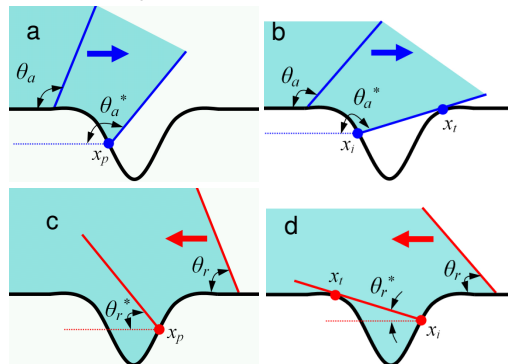


FIG. 1. Illustration of a contact line moving across a smooth defect. (a) The micro-meniscus of an advancing contact line (blue) does not touch the r.h.s. of the defect. (b) The micro-meniscus of an advancing contact line (blue) does touch the r.h.s. of the defect. (c) The micro-meniscus of a receding contact line (red) does not touch the l.h.s. of the defect. (d) The micro-meniscus of a receding contact line (red) does touch the l.h.s. of the defect.

If θ_r is large and/or the defect is shallow such that the micro-meniscus does not touch the opposite side of the defect (Fig 1(c)) then the *effective* receding contact angle introduced by the defect is given by $\theta_r^* = \theta_r - \tan^{-1}(h'(x_p))$ where x_p is the point of inflection on the r.h.s. of $h(x)$; the relationship between θ_r and θ_r^* is linear. Movement of the contact line past this point would result in instability as the local curvature of the liquid at the defect would be higher than the curvature of the droplet; this situation conflicts with the Young-Laplace equation [19,20] and would result in the microscopic contact

angle being greater than the macroscopic contact angle. The contact angle hysteresis of the defect $\Delta\theta^*$ is thus given by $\Delta\theta + 2\tan^{-1}(h'(x_p))$ where $\Delta\theta = \theta_a - \theta_r$; this is the contact angle hysteresis far from the defect.

If, however, as the contact line moves down the r.h.s. of the defect with the macroscopic contact angle reducing, the liquid meniscus touches the l.h.s. of the defect (at $x = x_i$) then in this case θ_r^* of the defect, which is given by $\tan^{-1}(h'(x_i))$, is equal to $\theta_r - \tan^{-1}(h'(x_i))$; the relationship between θ_r and θ_r^* is non-linear. This is the *tangent line* at x_i which also intersects $h(x)$ at $x = x_i$; this case was illustrated in Fig. 1(d). By symmetry, θ_a^* is given by $\theta_a - \tan^{-1}(h'(x_i))$ by using the same arguments above but with the contact line moving from left to right (Fig. 1(b)). Continuing the receding angle case, once the micro-meniscus touches the l.h.s. of the defect at x_i , it will break as the Young-Dupré equation [18,19] is not satisfied at x_i ; as a consequence the droplet will depin. As $h(x)$ is a smooth function, it follows that we should be able to predict the contact angle hysteresis introduced by the defect in terms of simple parameters (the defect depth h_0 , the defect width w and $\theta_{r,a}$). As a first approximation, since w and h_0 are much smaller than the droplet diameter (~ 1 mm) we can consider the profile of the micro-meniscus at the defect to be that of a straight line (although in reality it is a curve). Thus, the required tangent line cuts $h(x)$ at two points: the tangent point (x_i) on the l.h.s. of the defect and the intersection point (x_i) on the r.h.s. of the defect. Hence, we can write $\theta_{r,a}^* = \tan^{-1}(h'(x_i))$ and $\tan^{-1}(h'(x_i)) = \theta_{r,a} - \tan^{-1}(h'(x_i))$ together with the tangent line $h(x_i) - h(x_i) = h'(x_i)(x_r - x_i)$.

The micropatterned defects can be modeled using a cosine function over a single period: $h(x) = -\frac{1}{2}(\cos(2\pi x/w) + 1)$ where h_0 and w are described above. Two tangent line solutions exist for given values of θ_r and θ_a ; the required solution is the tangent line which intersects $h(x)$ above its point of inflection as this is where the micro-meniscus initially touches both sides of the defect simultaneously. A numerical solution to the equations above leads to the curves given in Fig. 2 which shows the calculated *effective* receding and advancing contact angles as a function of the receding and advancing contact angles.

Due to symmetry, the tangent line solution applies to both receding and advancing contact angles as $\theta_a^* = \pi - \theta_r^*$; note that this only holds for a defect which is symmetrical around $x = 0$. Note that Fig. 2 indicates that there can be two values of $\theta_{r,a}^*$ for a given $\theta_{r,a}$; the dashed lines correspond to the second tangent line solution and do not physically occur as the micro-meniscus touches the other side of the defect and depins at the first tangent line solution. It should also be noted that the solutions are *scale-independent*, i.e. a tangent line solution is true for *any* cosine function (defect) having a ratio $h_0/w = \kappa$ where κ is the *aspect ratio* of the defect, as shown in the inset of Fig. 2.

In order to test our model we fabricated micropatterned surfaces using the photoresist SU-8. A photolithographic mask enabled the formation concentric circles (trench-like defects) of diminishing diameters (0.1-2 mm), see Fig. 3. The surfaces

were also covered with a thin coating (~ 100 nm) of fluorocarbon (FC) [21] using a C_4F_8 plasma deposition (Surface Technology Systems, UK).

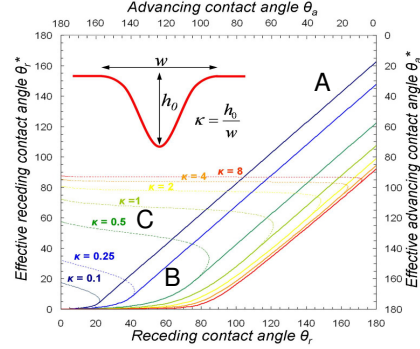


FIG. 2. Theoretical curves for the effective receding and advancing contact angles on defects of differing aspect ratio κ . The linear part (indicated by A) of the curve (slope = 1) corresponds to the case where the micro-meniscus does not touch the opposite side of the defect when moving across it. The non-linear part of the curve (indicated by B) corresponds to the first tangent line solution. The dashed non-linear part of the curve (indicated by C) corresponds to the second tangent line solution which is not physically observed here. Inset shows the dimensions of the defect: h_0 corresponds to the defect depth, w the width and κ the aspect ratio.

The measurements were performed in a class ISO 5/7 cleanroom ($T_A = 20^\circ\text{C} \pm 0.5^\circ\text{C}$; $RH = 45\% \pm 2\%$) using a contact angle meter (Kruss, Germany). Contact angle hysteresis was measured using droplet expansion (syringe pump) and evaporation [22-24]. In order to measure θ_a^* and θ_r^* using the syringe method, a small droplet of liquid ($vol \sim 0.3$ nL) was positioned onto the smallest concentric circle ($\phi = 100$ μm) at the centre of the micropatterned surface and swelled using a syringe pump ($1-5$ $\mu\text{L min}^{-1}$). Once the droplet diameter was larger than the largest concentric circle in the micropattern ($\phi = 2$ mm), the droplet volume was reduced using the syringe ($1-5$ $\mu\text{L min}^{-1}$) in order to measure θ_r^* . For the evaporation tests, a droplet ($vol \sim 2$ μL) was placed on the micropatterned surface and allowed to slowly evaporate (unforced) whilst the value of θ_r^* was recorded as a function of time. This evaporation method was not possible for ethylene glycol due to a low vapor pressure at room temperature [25]; however, evaporation tests were possible using IPA/ H_2O solutions as the vapor pressure of IPA and of water are very similar at room temperature [25].

Fig. 3(a) shows a typical droplet evaporation sequence recorded for a micropattern. The droplet evaporates until it becomes pinned onto a circular defect ($t = 431$ s). The apparent contact angle reduces until the effective contact angle is attained whereby the droplet suddenly depins ($t = 661$ s) and pins to the subsequent circle defect, the process repeats one more time. Fig. 3(b) shows data gathered over a period of 375 s for an evaporating droplet (IPA/ H_2O : 2.5/97.5) on a FC coated SU-8 surface containing smooth

defect concentric circles spaced by 100 μm . Two distinct phases are apparent: Phase (i) corresponds to droplet evaporation at constant contact angle with diminishing droplet base radius [23] when the droplet is not pinned to a defect and phase (ii) involves an evaporating droplet depinning from circle defect to circle defect. The droplet depinning is described by the equation in Fig. 3(b). However, between depinnings, which occurs very quickly (<200 ms) at constant volume (cf. Fig. 3(a)) the evaporation is described as in Ref. [23]. The model presented here (see Fig. 2) predicts the depinning contact angle θ_r^* ; we now test this model with various liquids.

Fig. 4 shows a plot of the experimentally obtained values of θ_r^* and θ_a^* as a function of θ_r and θ_a for various liquids on surfaces containing smooth micropatterned defects. Our measurements indicate that the model can accurately predict the values of θ_r^* introduced by the defect thus giving strong evidence for the tangent line solution model for the contact angle hysteresis introduced by a smooth defect. Fig. 4(a) indicates that there are six points lying on the non-linear solution and one point (red circle) on the linear solution. The inset to Fig. 4(a) illustrates good agreement between the experimental defect and the model. Despite the defect not being a perfect cosine shape the parameters h_0 and w enable a good fit between the real defect shape and the model in the region where the liquids depin.

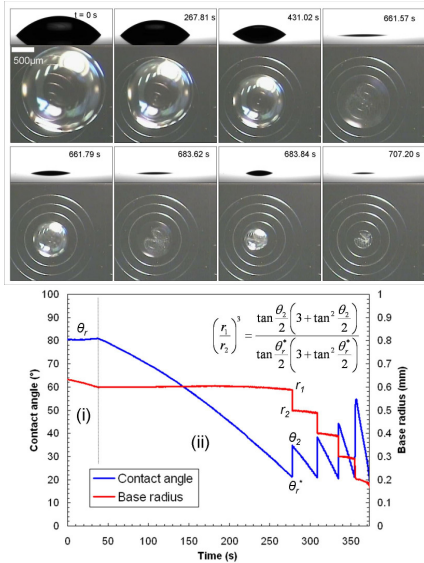


FIG. 3. (a) Plan and side view optical images of a liquid droplet (H_2O) evaporation sequence taken over 707 s on a micropatterned surface (SU-8) composed of concentric circle defects separated by 200 μm . (b) Variation of contact angle (red line) and droplet base diameter (blue line) as a function of time for a IPA/ H_2O ($\text{vol/vol} = 2.5/97.5$) droplet on smooth defects separated by 100 μm defined in SU-8 covered with FC.

Let us now consider the experimental results for θ_a^* shown in Fig. 4(b). Due to the finite needle diameter the values of θ_a^* were measured at droplet base radii between 0.5-1 mm. Two

liquid/surface combinations fit very well with the predictions of the model and five deviate from the model. In order to explain this, horizontal colored bars have been added to Fig. 4(b) which indicate the value of contact angle calculated using a base radius r of 0.75 mm and equating the droplet diameter D to the capillary length $(\gamma/\rho g)^{1/2}$ of the liquid. These bars represent the point where gravity can no longer be considered to be negligible; droplets can vibrate [26] leading to possible depinning [27] before the tangent line solution. To illustrate this another way, in order to observe $\theta_a^* = 175.3^\circ$, as predicted by the model, then a droplet of ethylene glycol (on a FC covered defect, $r = 0.75$ mm, $\gamma = 47.7$ mJ m^{-2} , $\rho = 1096.8$ kg m^{-3} [25]) would need to be swelled to a diameter of 18.3 mm.

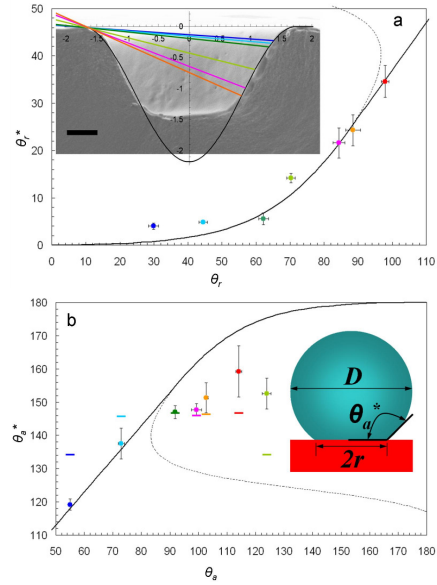


FIG. 4. Experimental values of the effective receding and advancing contact angles on a defect for various liquids. (a) The effective receding contact angle (θ_r^*). H_2O on SU-8 (dark green circle), H_2O on FC (red circle), $\text{C}_2\text{H}_6\text{O}_2$ on SU-8 (dark blue circle), $\text{C}_2\text{H}_6\text{O}_2$ on FC (light green circle), IPA/ H_2O (2.5/97.5) on FC (orange circle), IPA/ H_2O (5/95) on FC (pink circle) and IPA/ H_2O (10/90) on SU-8 (light blue circle). The predicted curve (black) using the model is also shown (using an aspect ratio $\kappa = 0.625$). Inset shows an SEM image of a cross-section of a defect formed using photolithography of SU-8 (the 100 nm thick fluorocarbon layer deposited onto the SU-8 surface is visible) superimposed with the model cosine curve with $\kappa = 0.625$. The colored lines represent the tangent line solutions for the various liquids; the color of the lines corresponds to the code above. (b) The effective advancing contact angle (θ_a^*) on a defect using the same color code as above. The predicted curve (black) using the model is also shown (using an aspect ratio $\kappa = 0.625$). The colored bars (same color code as above) represent the calculated contact angle when the droplet diameter is equal to the capillary length of the liquid. Inset show a droplet resting on a solid surface, $D = 2r/\sin(\pi - \theta_a^*)$.

As a summary, the table shows the receding contact angle θ_r and the advancing contact angle θ_a on SU-8 and C_4F_8 treated

SU-8 with and without the presence of smooth defects using deionized water (DI-H₂O), isopropyl alcohol (IPA) [VLSI grade, Carlo Erba Reagents, Italy]/DI-H₂O solutions (*vol/vol* = 2.5/97.5, 5/95 and 10/90) and ethylene glycol (C₂H₆O₂) [Reagent grade, Scharlau, Spain]. The experimental values were obtained using tilt and syringe (contraction and expansion) and methods. All measurements were conducted at least 5 times.

Although the lithographically micropatterned defects are larger than the natural surface defects, which are on the nanometer scale, we believe that understanding the behavior of these smooth simple defects could lead to a better understanding of contact angle hysteresis inherent to natural surfaces due to the *scale-independence* of the solution. Finally, the idea proposed here could be extended to periodic surfaces, e.g. hydrophobic surfaces, or even more complicated surfaces where, e.g. the function $h(x)$ is not symmetrical around $x = 0$, thus leading to complex wetting and dewetting of surfaces, i.e. a tunable contact angle hysteresis tailored to ones needs.

*steve.arscott@iemn.univ-lille1.fr

- [1] R. N. Wenzel, *Ind. Eng. Chem.* **28**, 988 (1936).
 [2] A. B. D. Cassie and S. Baxter, *Trans. Faraday Soc.* **40**, 546 (1944).
 [3] C. Huh and S.G. Mason, *J. Colloid and Interface Sci.* **60** 11 (1977).
 [4] P. G. De Gennes, *Rev. Mod. Phys.* **57**, 827 (1985).
 [5] A. Lafuma and D. Quéré, *Nature Materials* **2**, 457 (2003).
 [6] C. Neinhuis and W. Barthlott, *Annals of Botany* **79**, 667 (1997).
 [7] X. F. Gao and L. Jiang, *Nature* **432**, 36 (2004).
 [8] Y. Zheng, H. Bai, Z. Huang, X. Tian, F-Q Nie, Y. Zhao, J. Zhai, and L. Jiang, *Nature* **463** 640 (2004).

- [9] L. Feng, *et al. Adv. Mater.* **14**, 1857 (2002).
 [10] F.E. Bartell and J.W. Shepard, *J. Phys. Chem.* **57**, 455 (1953).
 [11] R. E. Johnson and R. H. Dettre *J. Phys. Chem.* **68**, 1744 (1964).
 [12] J. F. Joanny and P. G. De Gennes *J. Chem. Phys.* **81**, 552 (1984).
 [13] Y. L. Chen, C. A. Helm, and J. N. Israelachvili *J. Phys. Chem.* **95**, 10736 (1991).
 [14] R. Blossey, *Nature Mater.* **2**, 301 (2003).
 [15] D. J. Harrison, K. Fluri, K. Seiler, Z. Fan, C. S. Effenhauser, and A. Manz, *Science* **261**, 895 (1993).
 [16] G. M. Whitesides and B. Grzybowski, *Science* **295**, 2418-2421 (2002).
 [17] J. B. Hannon, S. Kodambaka, F. M. Ross, and R. M. Tromp, *Nature* **440**, 69 (2006).
 [18] T. Young, *Philos. Trans. Soc. London*, **95**, 65 (1805).
 [19] *Capillarity and Wetting Phenomena: Drops, Bubbles, Pearls, Waves*, P.G. de Gennes, F. Brochard-Wyart and D. Quéré, Springer Science, USA (2003).
 [20] P-S de Laplace, *Œuvres complètes de Laplace*, t. IV, supplément au livre X du traité de la mécanique céleste, p. 394 – 2^e supplément au livre X, p. 419, Ch. I. (in French).
 [21] K. Takahashi and K. Tachibana, *J. App. Phys.* **89**, 893 (2001).
 [22] I. Langmuir, *Phys. Rev.* **12**, 368 (1918).
 [23] R. G. Picknett and R. Bexon, *J. Colloid Interface Sci.* **61**, 336 (1977).
 [24] R. D. Deegan, O. Bakajin, T. F. Dupont, G. Huber, S. R. Nagel, and T. A. Witten, *Nature* **389**, 827 (1997).
 [25] *CRC Handbook of Chemistry and Physics*, 69th Edition, Edited by R. C. Weast, CRC Press, Florida, USA.
 [26] Lord Rayleigh, *Proc. R. Soc. London*, **29**, 71 (1879).
 [27] S. Daniel, M. K. Chaudhury and P.G. de Gennes, *Langmuir*, **21**, 4240 (2005).

Liquid	Experimental receding and advancing contact angles				Model	
	θ_r	θ_a	θ_r^*	θ_a^*	θ_r^*	θ_a^*
H ₂ O ^(a)	62.2°±2.8°	91.8°±0.5°	5.6°±1.3°	147°±2°	6.8	154.7
H ₂ O ^(b)	97.9°±2.3°	114.1°±2.1°	34.6°±3.4°	159.3°±7.7°	35.0	171.6
C ₂ H ₆ O ₂ ^(a)	29.9°±1.5°	55°±0.6°	4°±0.7°	119.2°±1.7°	0.8	118.0
C ₂ H ₆ O ₂ ^(b)	70.2°±1.3°	123.9°±1.5°	14.2°±1°	152.6°±4.7°	10.7	175.3
IPA/H ₂ O (2.5/97.5) ^(b)	88.5°±4.3°	102.7°±1.4°	24.3°±3.3°	151.3°±4.5°	25.5	164.5
IPA/H ₂ O (5/95) ^(b)	84.3°±1.8°	98.3°±1°	21.6°±3.2°	147.7°±1.8°	21.3	161.0
IPA/H ₂ O (10/90) ^(a)	44.5°±1.2°	72.9°±1.1°	4.9°±0.1°	137.6°±4.6°	2.3	135.9

Table. Experimental values for receding contact angle (θ_r) and advancing contact angle (θ_a) for liquids on SU-8^(a) and SU-8 coated with a fluorocarbon (FC) layer^(b). The values were obtained using tilt and syringe methods using a DSA100 contact angle meter (Kruss, Germany). Table also shows Experimental values for the effective receding contact angle (θ_r^*) and effective advancing contact angle (θ_a^*) for various liquids on SU-8 and SU-8 coated with a fluorocarbon (FC) surfaces containing defects. The values were obtained using syringe and evaporation methods. Also shown are values predicted by the model (using $\kappa = 0.625$).